# Supporting Information

Polymorphism-induced multi-functional crystal photonics achieved by a highly luminescent benzofuranyl molecule having tetrafluorophenylene core

Takumi Matsuo,*[a,b] and Shotaro Hayashi*[a,b]

*a: School of Engineering Science, Kochi University of Technology, Kami, Kochi 782-8502, Japan.*

*b: FOREST Center, Research Institute, Kochi University of Technology, Kami, Kochi 782-8502, Japan.*

E-mail: hayashi.shotaro@kochi-tech.ac.jp; matsuo.takumi@kochi-tech.ac.jp

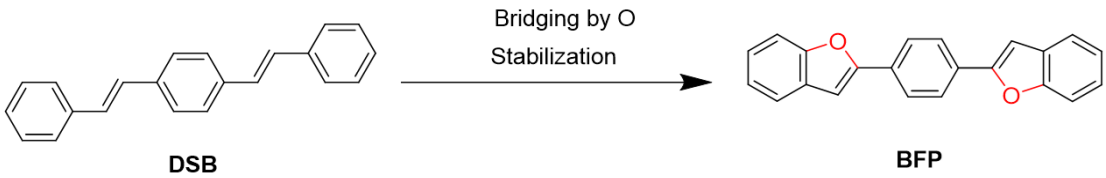


Scheme S1. A schematic depiction of design strategy of **BFP**.

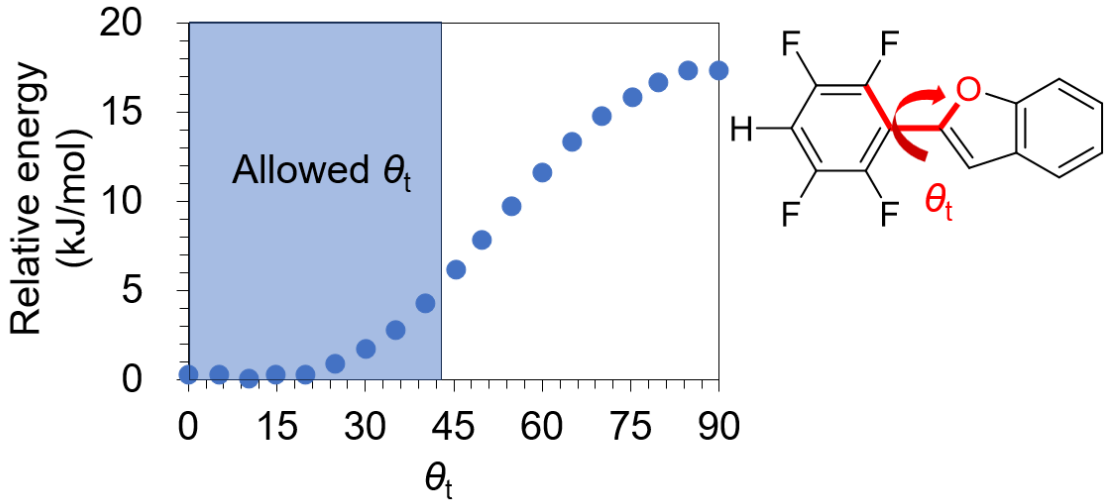


Scheme S2. Relative energy calculation for the model structure at each $\theta_t$. The inset exhibits the molecular structure model.

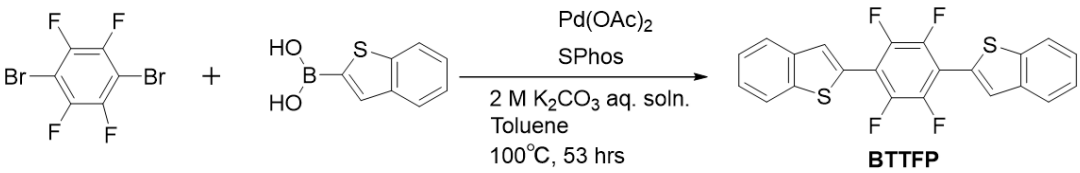


Scheme S3. Synthesis of **BTTFP**.

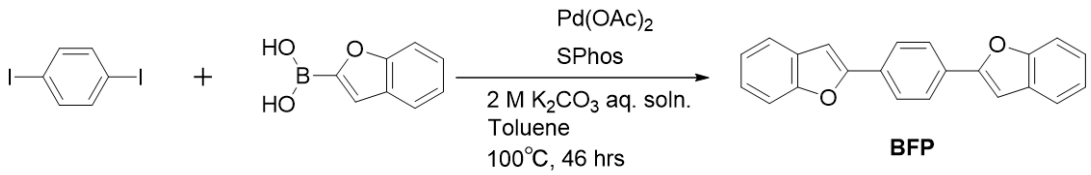


Scheme S4. Synthesis of **BFP**.

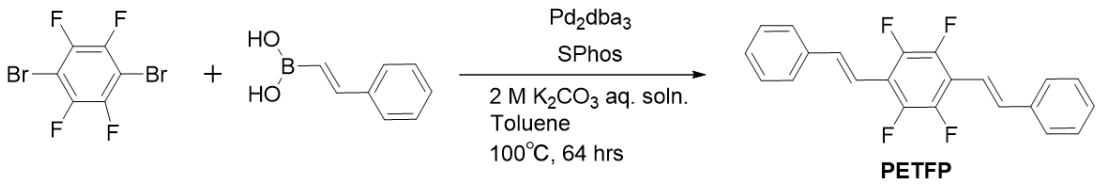


Scheme S5. Synthesis of **PETFP**.

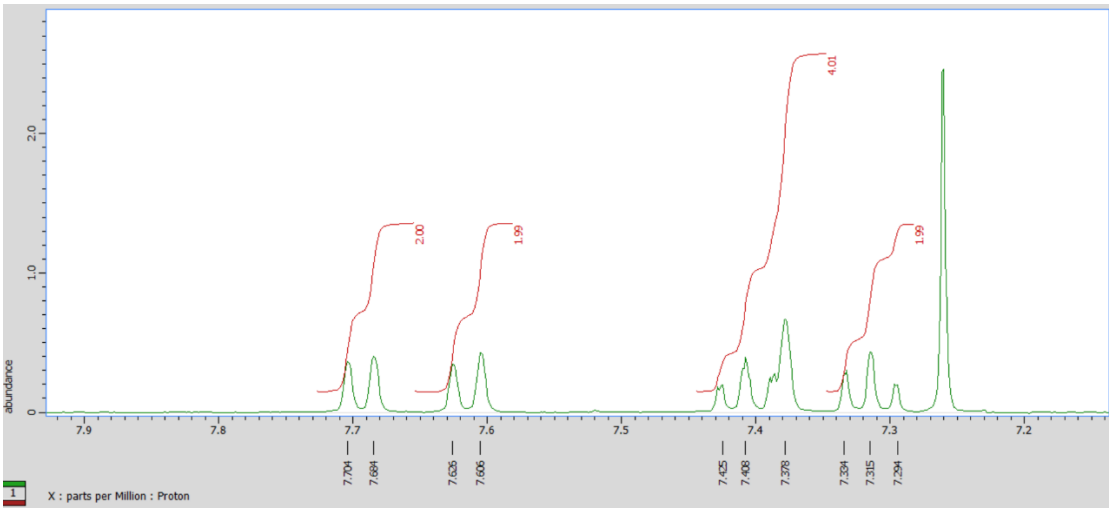


Figure S1. $^{1}$H-NMR spectrum measured for **BFTFP**.

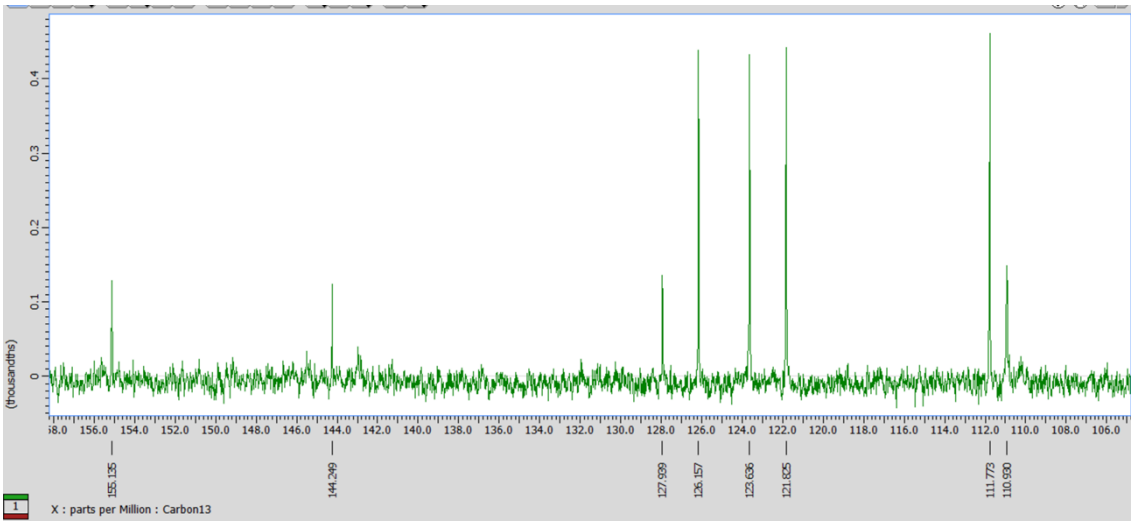


Figure S2. $^{13}$C-NMR spectrum measured for **BFTFP**.

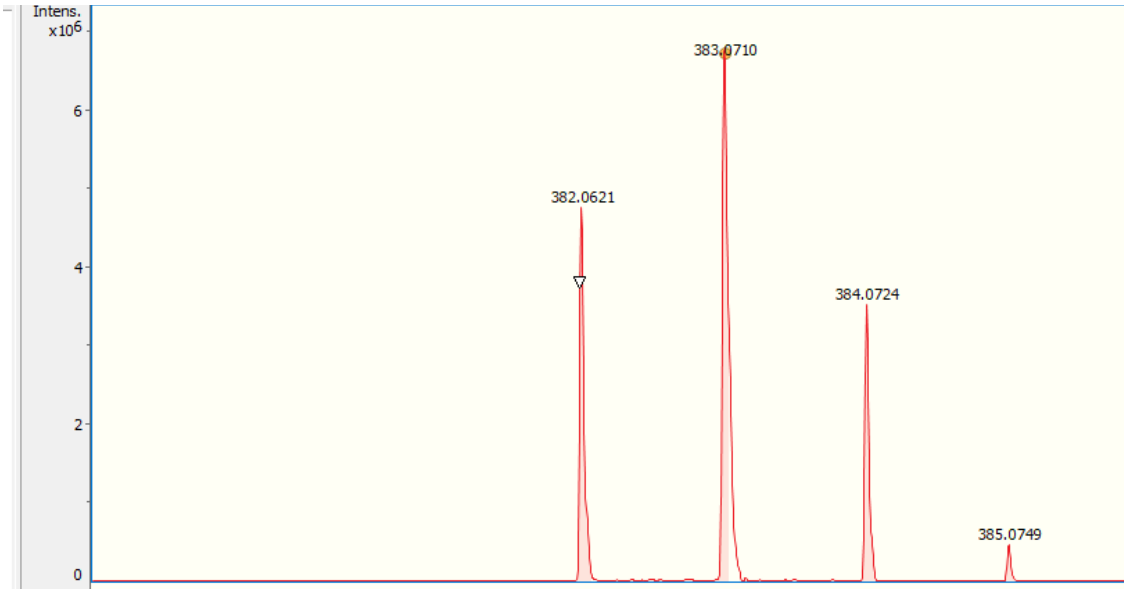


Figure S3. HR-MS spectrum measured for **BFTFP**.

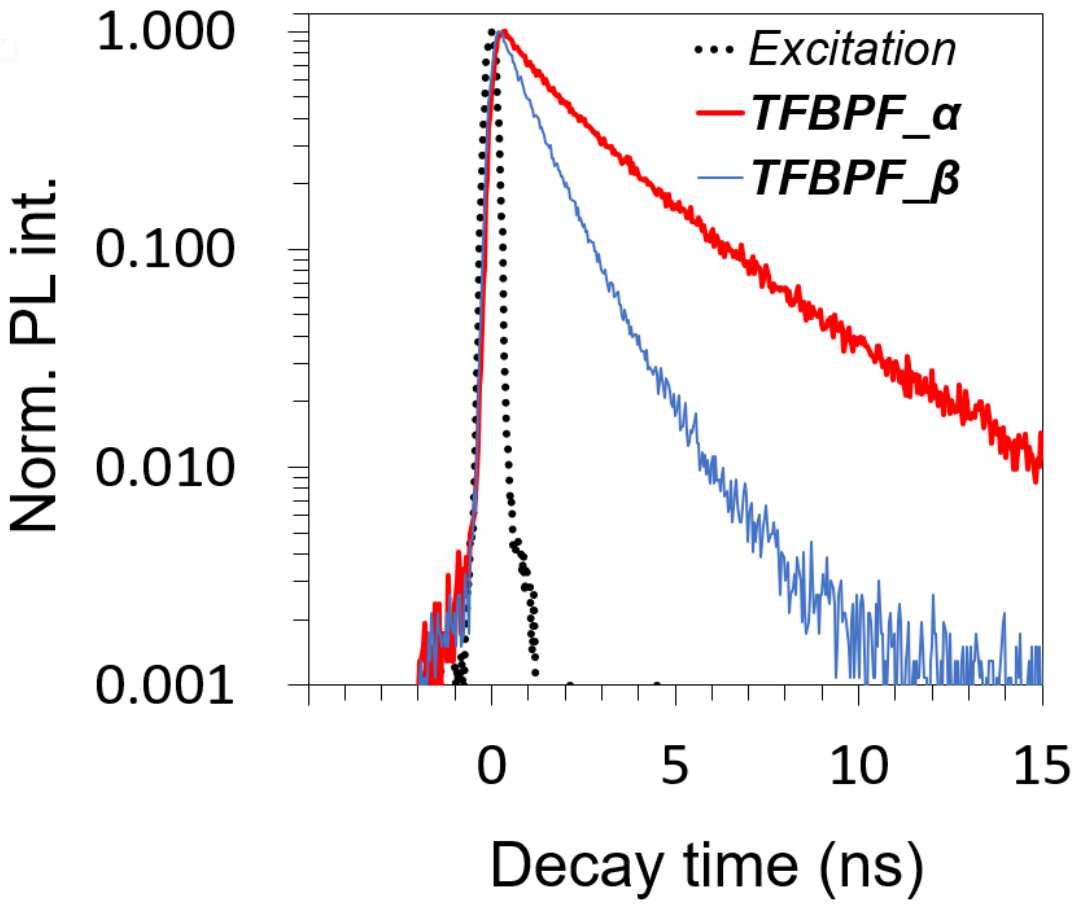


Figure S4. PL decay profiles measured for **BFTFP_*α*** and **BFTFP_*β***.

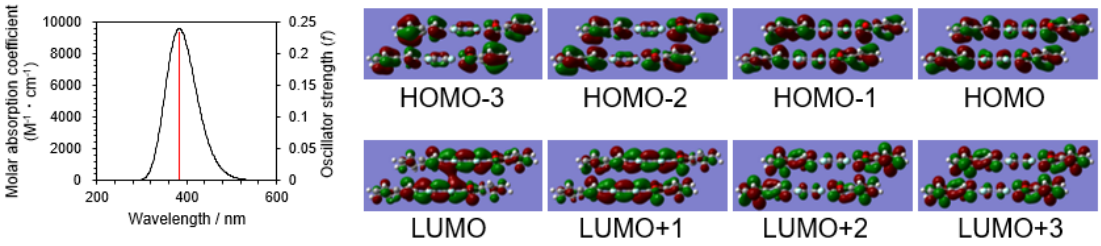


Figure S5. TD-DFT calculation for **BFTFP_α** (Isovalue: 0.02).

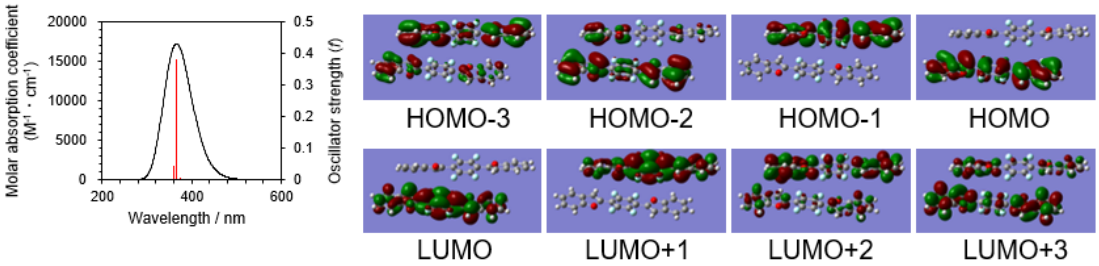


Figure S6. TD-DFT calculation for **BFTFP_*β*** (Isovalue: 0.02).

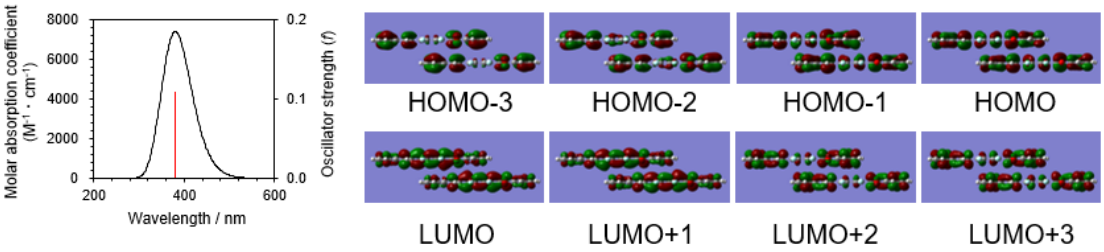


Figure S7. TD-DFT calculation for **BFTFP_*γ***_conformation1 (Isovalue: 0.02).

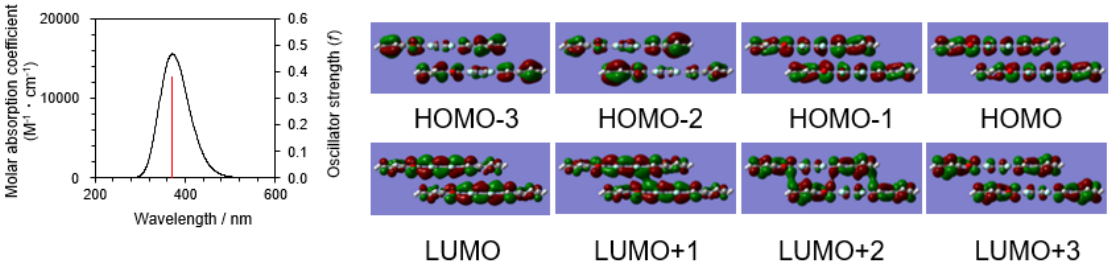


Figure S8. TDDFT calculation for **BFTFP_*γ***_conformation2. (Isovalue: 0.02).

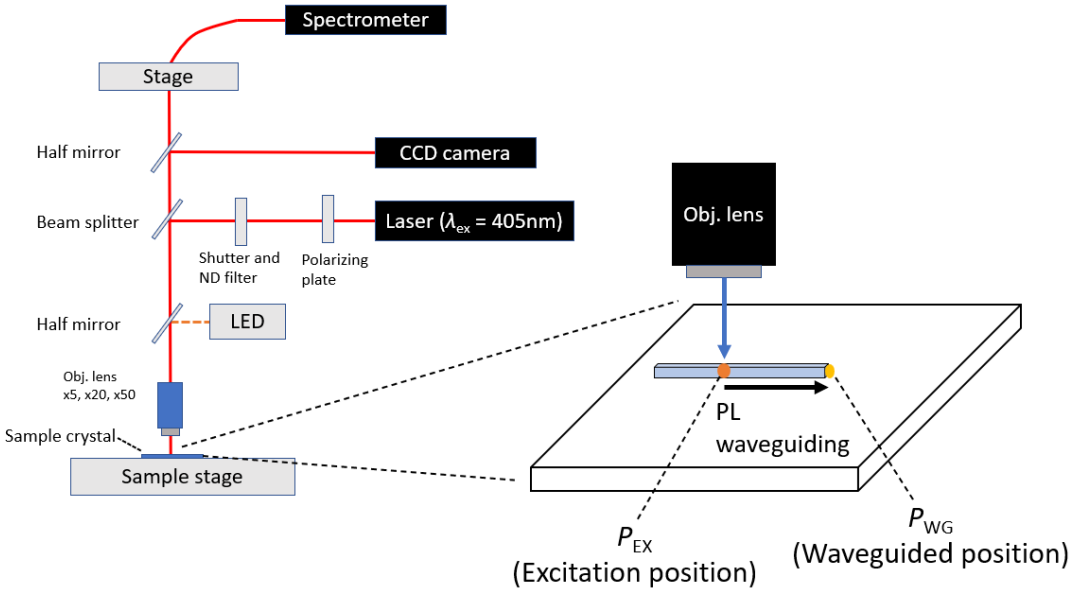


Figure S9. Schematic depiction of the set-up for spatially resolved μ-PL measurements.

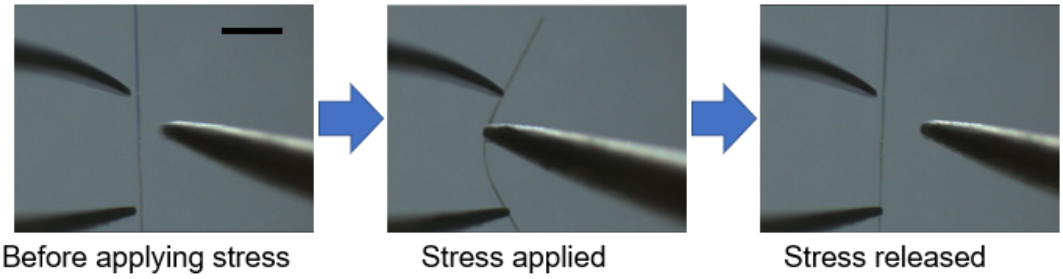


Figure S10. Bending examination performed for an isolated crystal of **BFTFP_*α***. Scale bar: 500 μm.

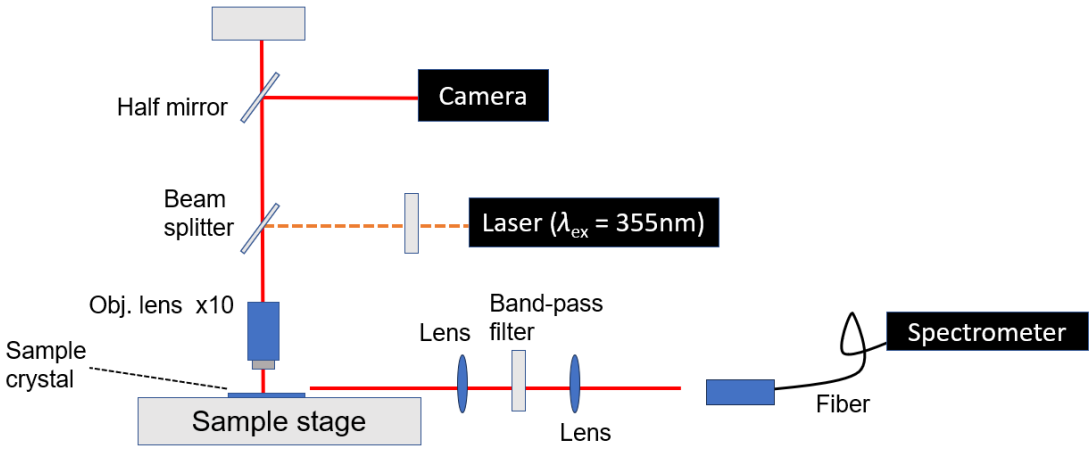


Figure S11. Schematic depiction of the set-up for measurements of ASE spectra.

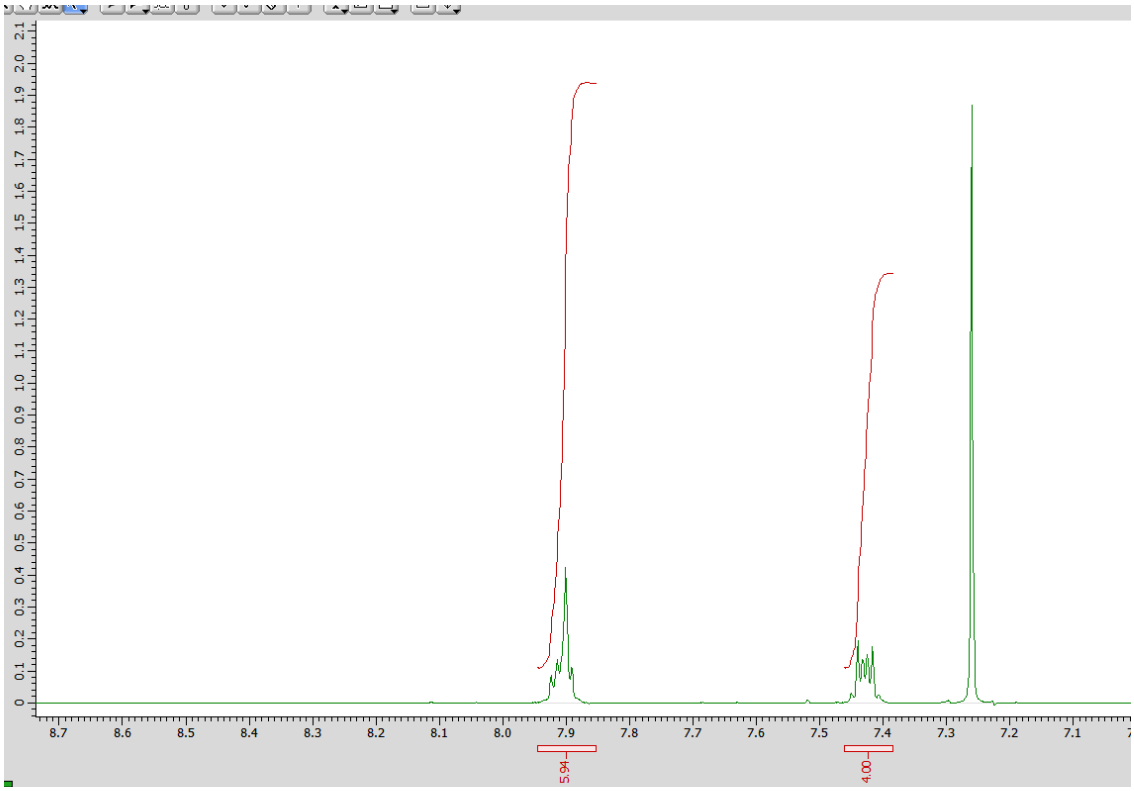


Figure S12. $^{1}$H-NMR spectrum measured for **BTTFP**.

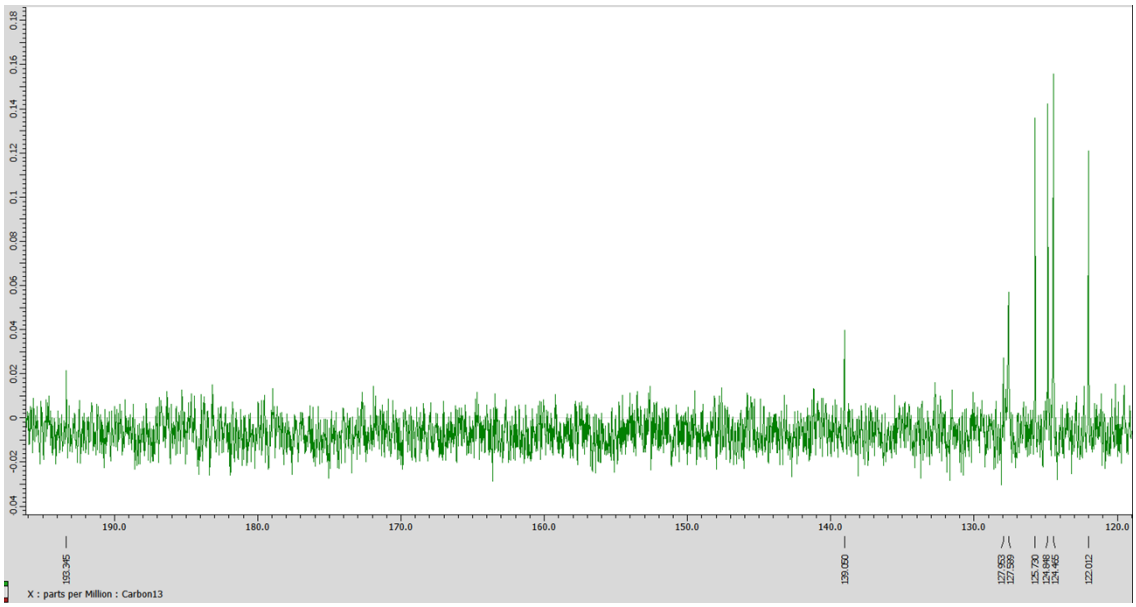


Figure S13. 13C-NMR spectrum measured for **BTTFP**.

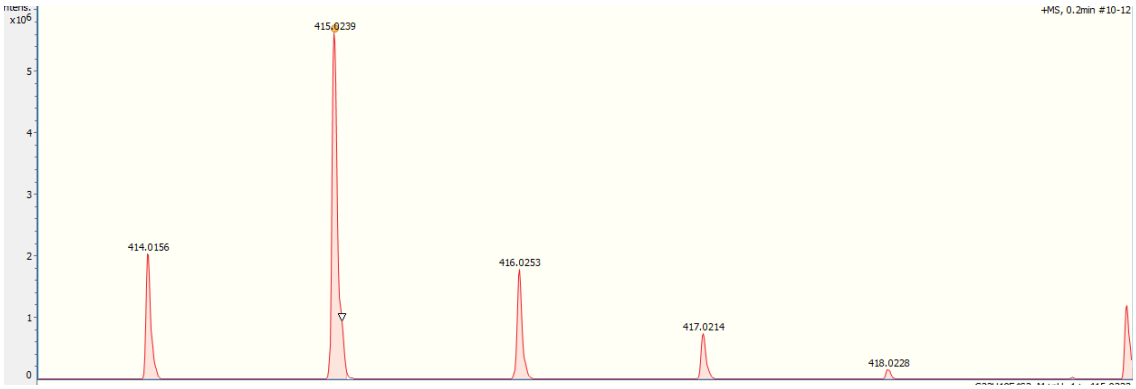


Figure S14. HR-MS spectrum measured for **BTTFP**.

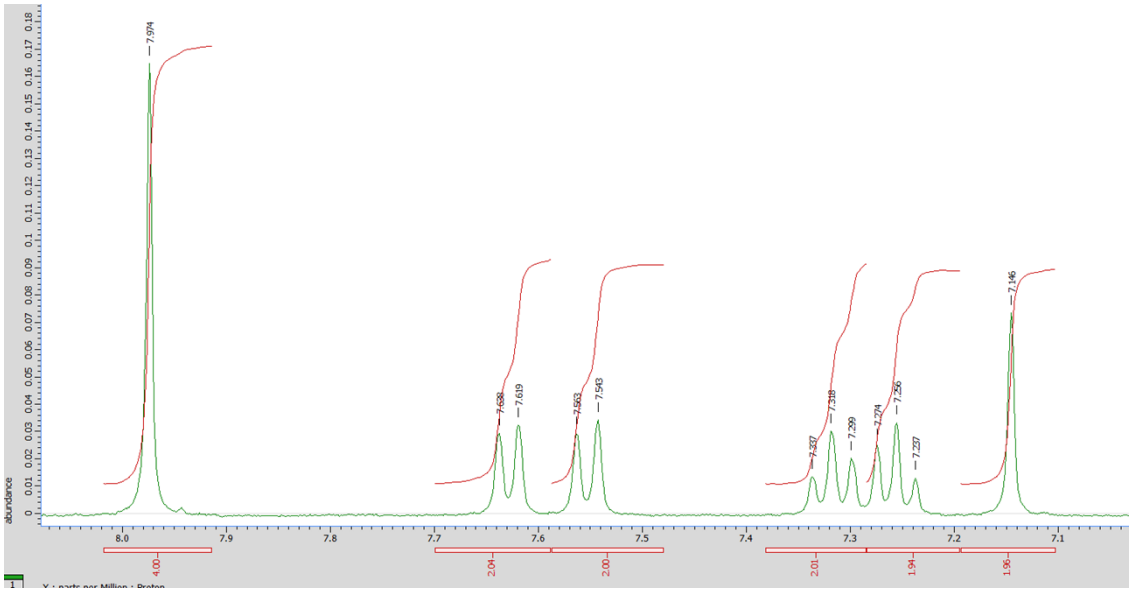


Figure S15. $^{1}$H-NMR spectrum measured for **BFP**.

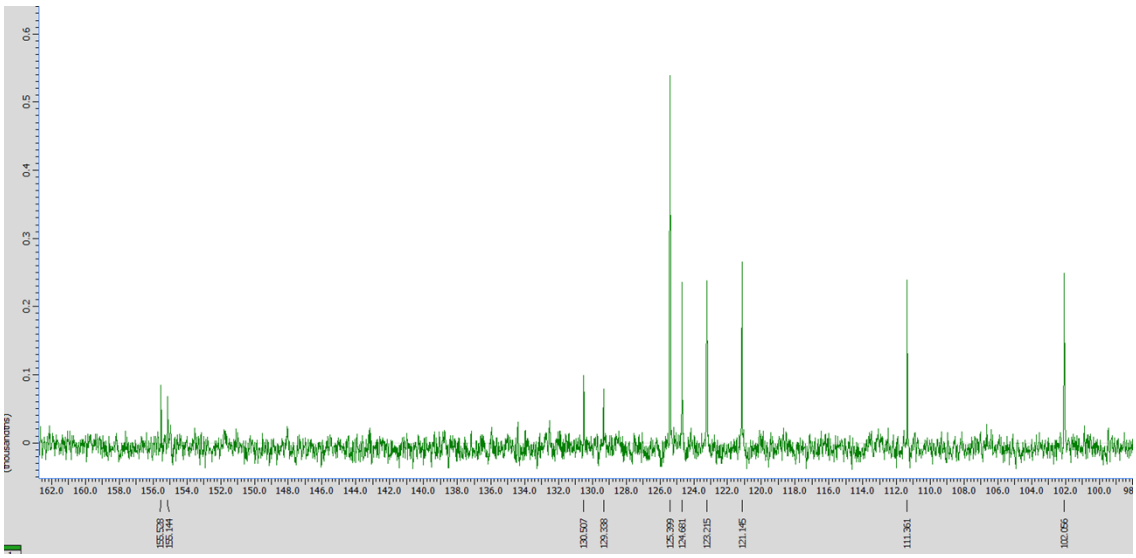


Figure S16. $^{13}$C-NMR spectrum measured for **BFP**.

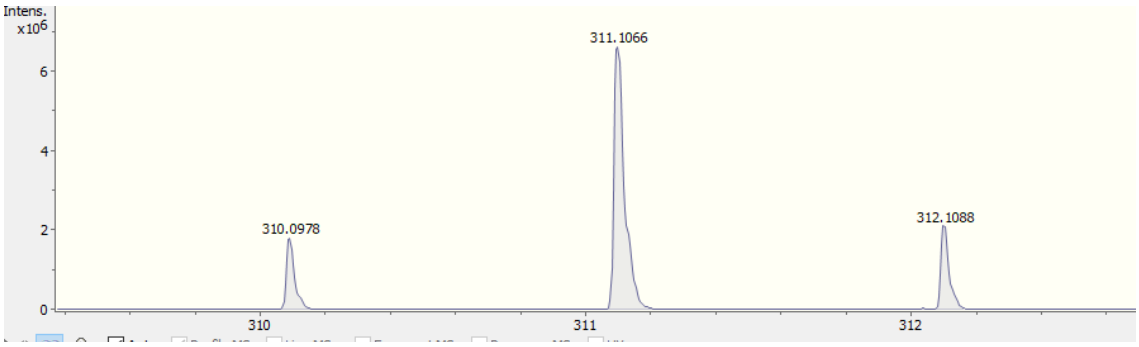


Figure S17. HR-MS spectrum measured for **BFP**.

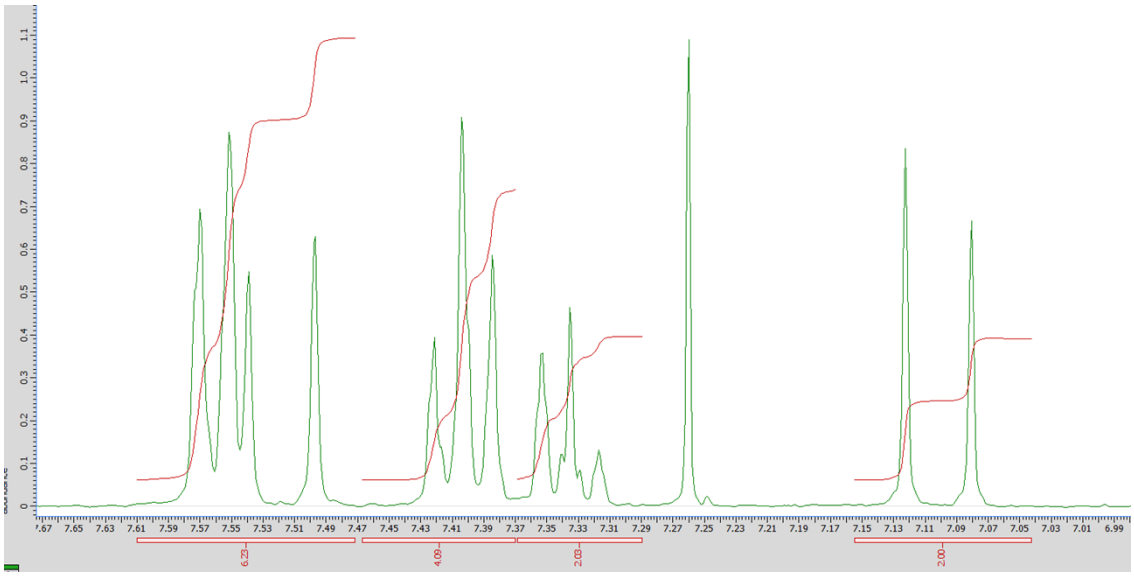

Figure S18. $^{1}$H-NMR spectrum measured for **PETFP**.

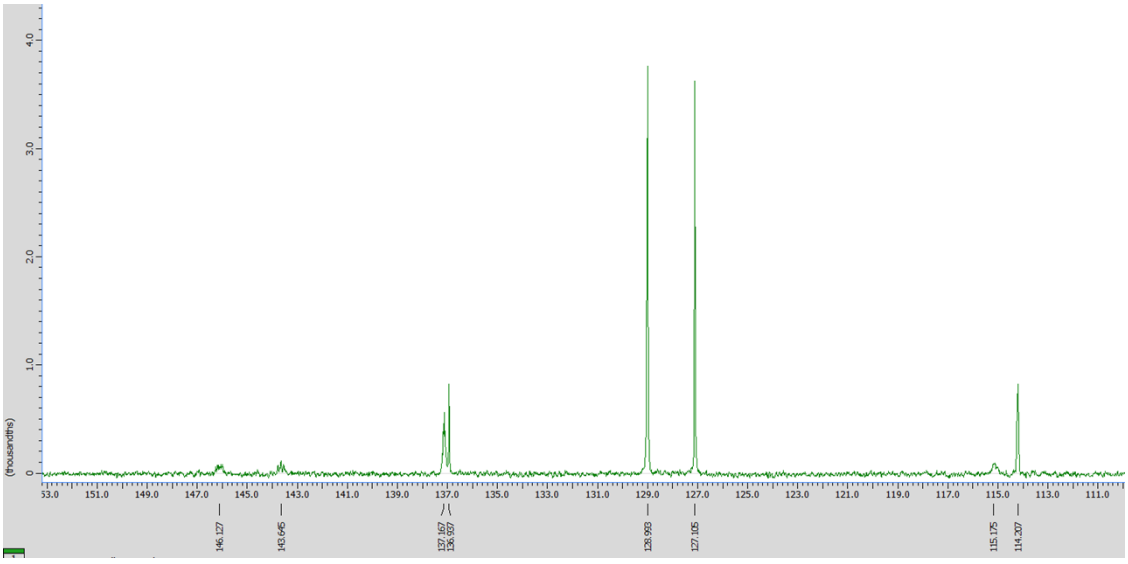


Figure S19. $^{13}$C-NMR spectrum measured for **PETFP**.

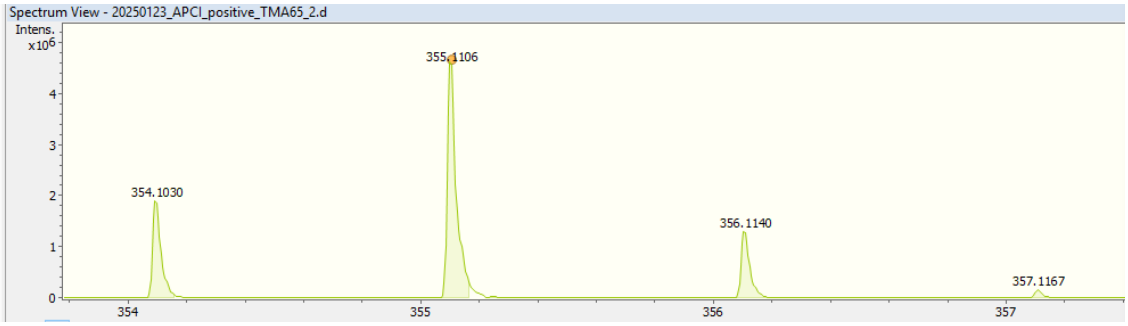


Figure S20. HR-MS spectrum measured for **PETFP**.

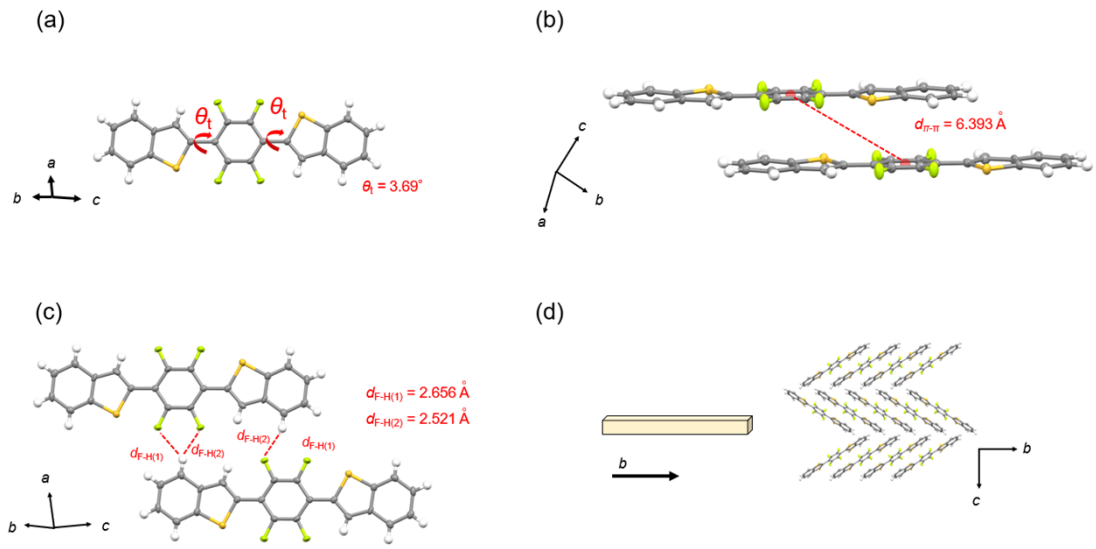


Figure S21. Crystal structure of **BTTFP**.

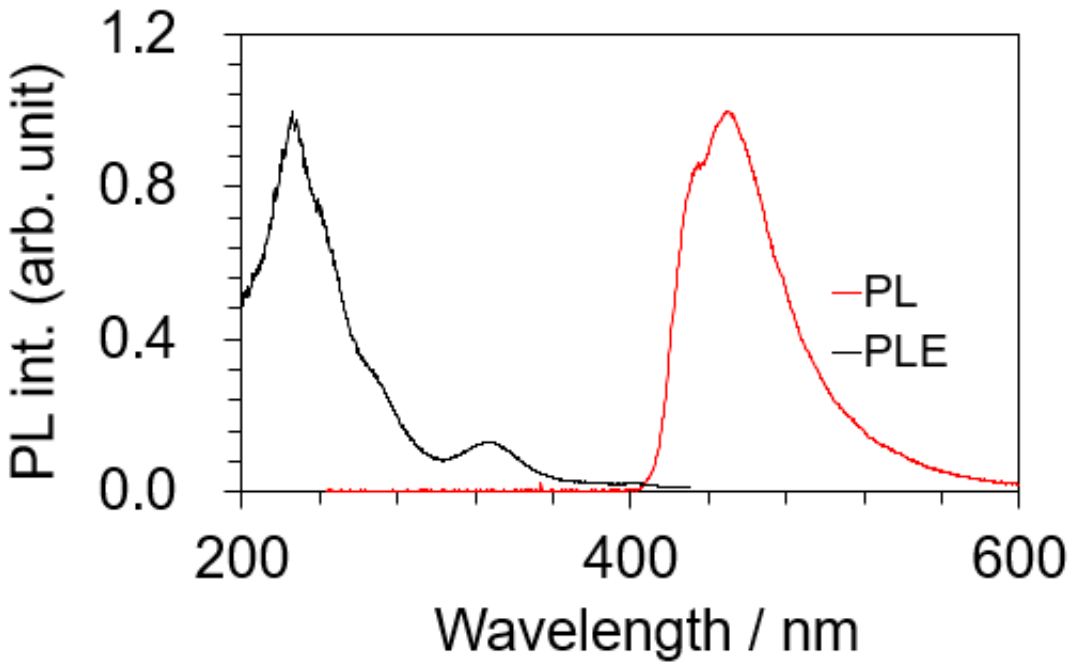


Figure S22. PL and PLE spectra measured for **BTTFP** monitored at 450nm.

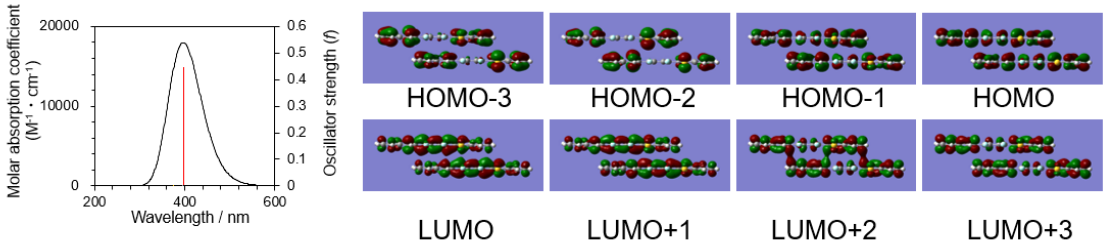


Figure S23. TDDFT calculation for **BTTFP** (Isovalue: 0.02).

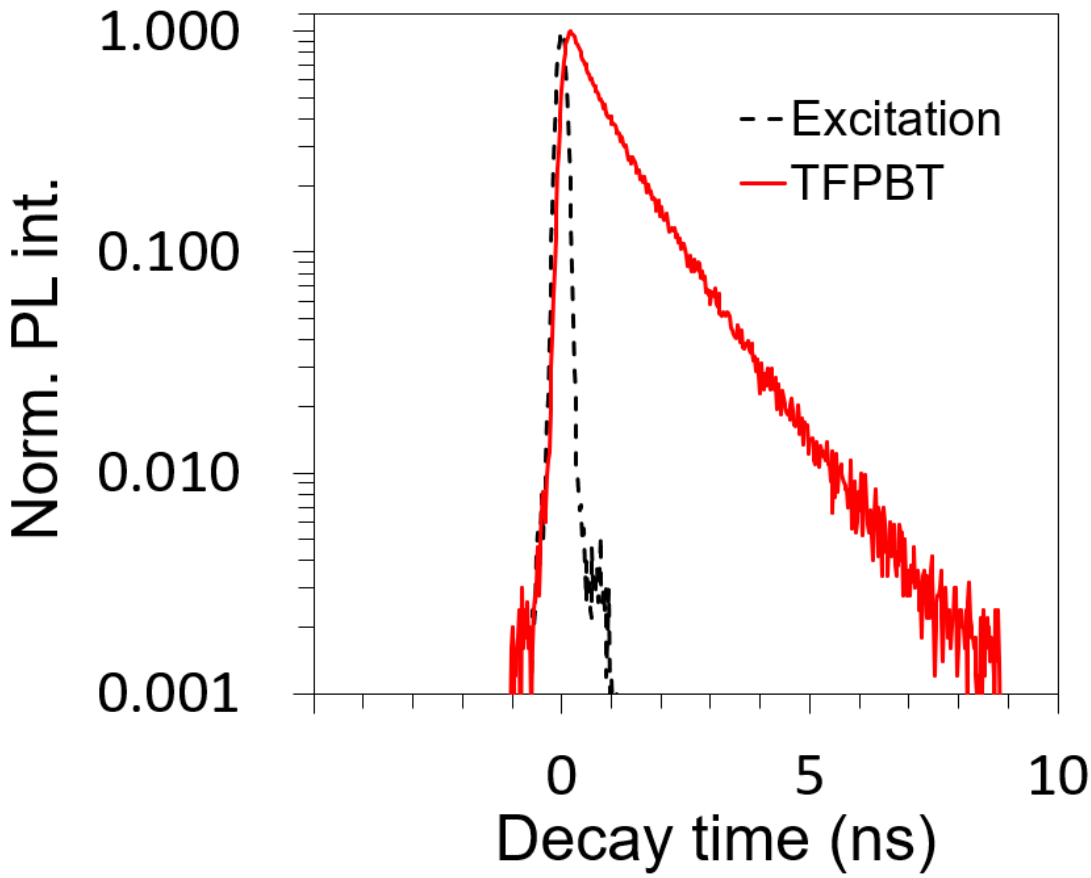


Figure S24. PL lifetime measured for crystals of **BTTFP**.

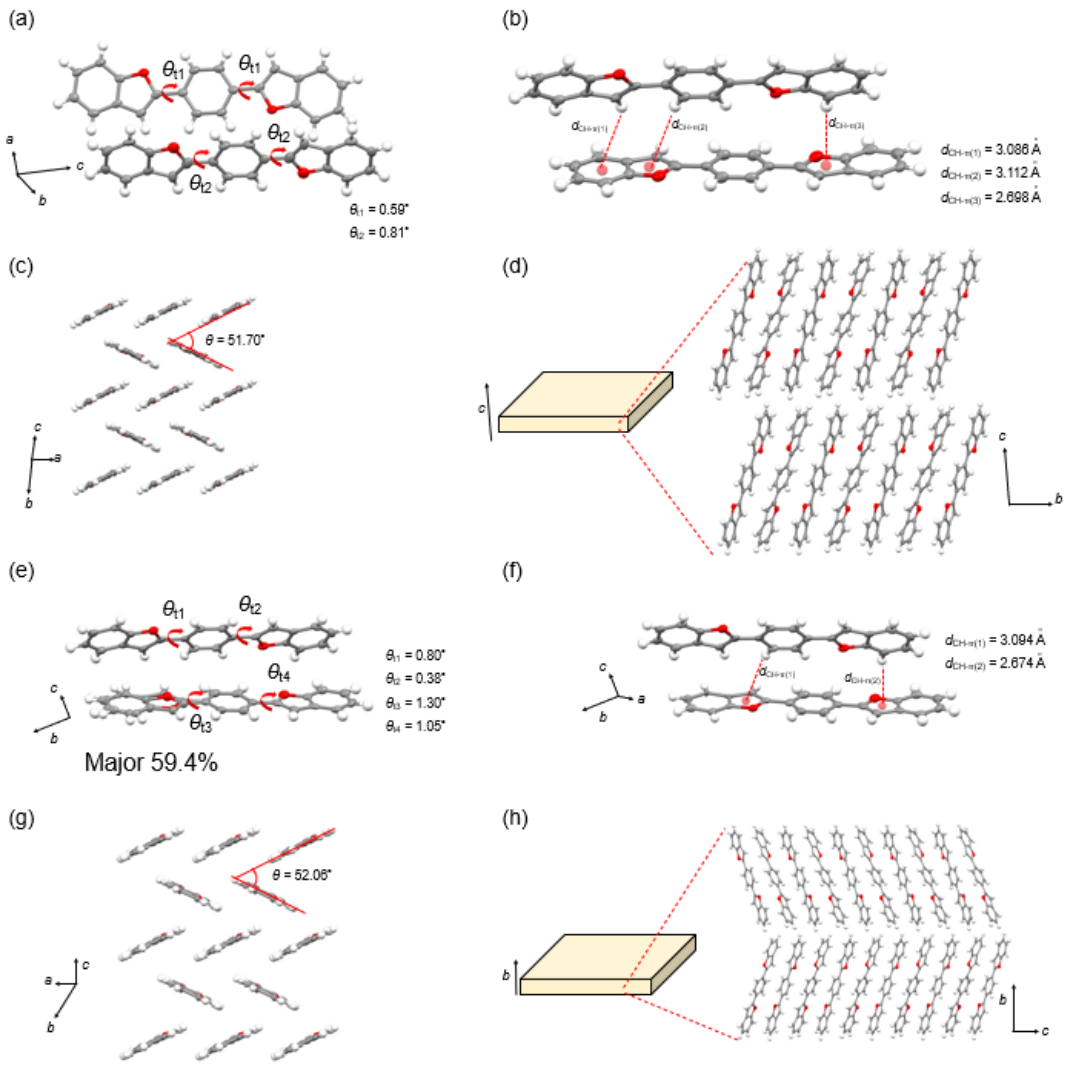


Figure S25. Crystal structure of **BFP**.

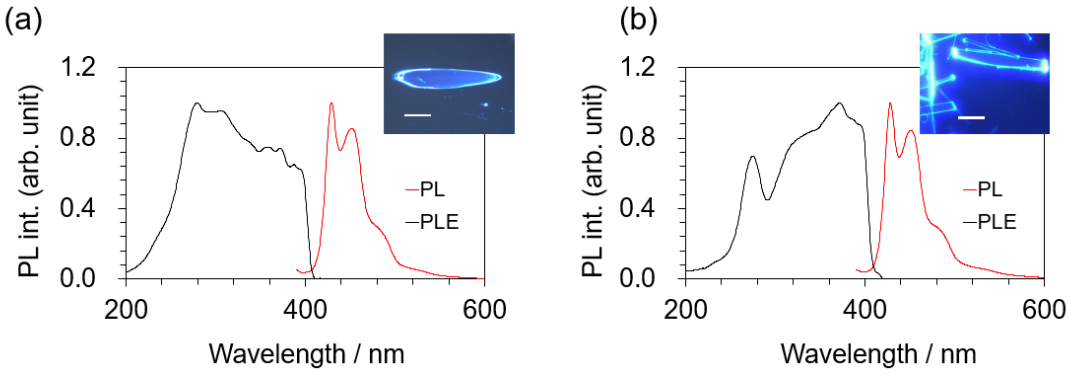


Figure S26. PL and PLE spectra measured for (a) **BFP_*α*** and (b) **BFP_*β***, respectively. Each inset shows the PL microscope image. Each scale bar: 2 mm and 100 μm, respectively.

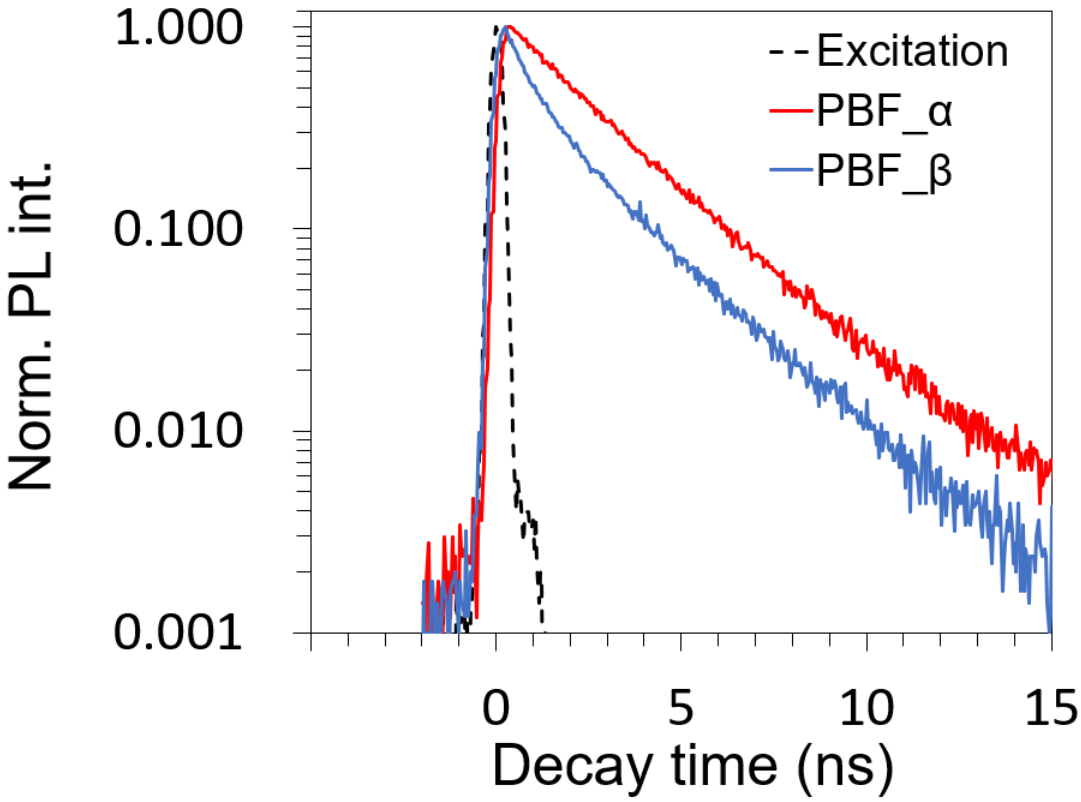


Figure S27. PL lifetime measured for (a) **BFP_*α*** and (b) **BFP_*β***, respectively.

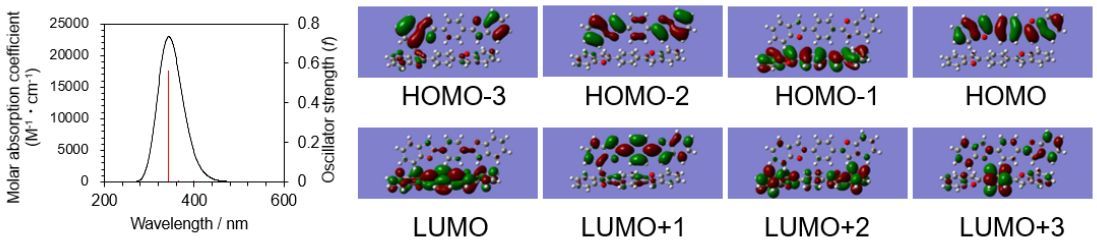


Figure S28. TDDFT calculation for **BFP_*α*** (Isovalue: 0.02).

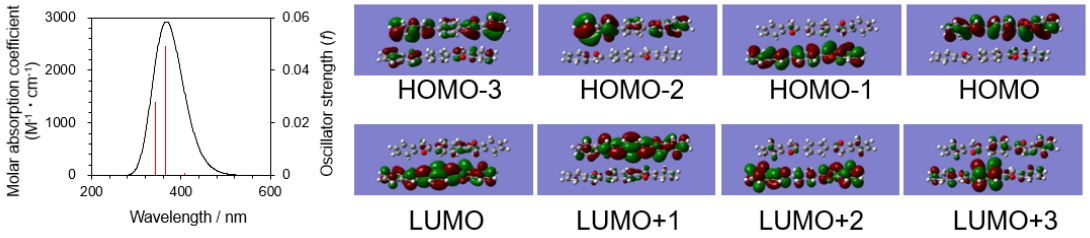


Figure S29. TDDFT calculation for **BFP_*β*** (Isovalue: 0.02).

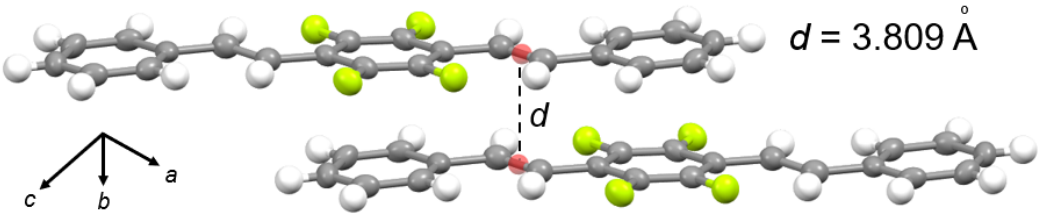


Figure S30. Crystal structure revealed for **PETFP**.

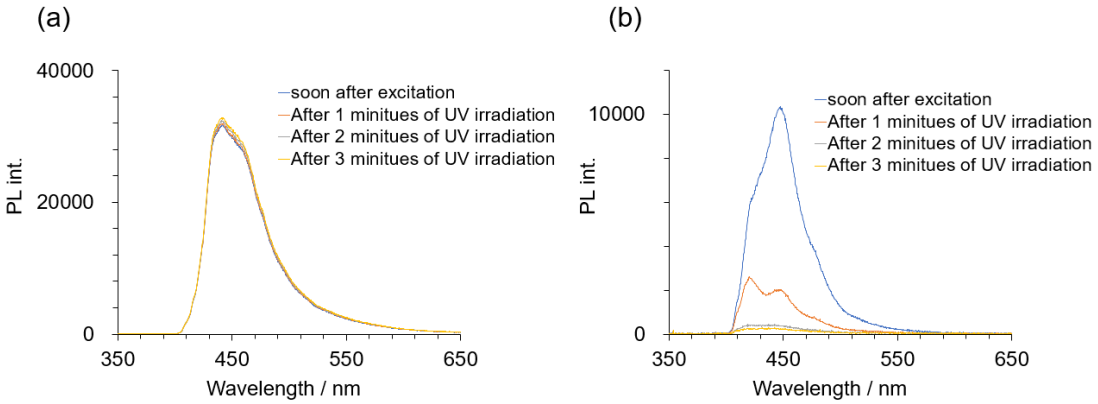


Figure S31. PL spectra at each UV irradiation time measured for an isolated crystal of (a) **BFTFP_*α*** and (b) **PETFP**, respectively.

Table S1. Excited state energy levels and orbital transitions calculated for a model of **BFTFP_*α***.

| States | Energy / eV | λ / nm | *f* / - | Orbital transitions | CI coefficient |
|---|---|---|---|---|---|
| S1 | 3.2347 | 383.29 | 0.2321 | HOMO-1→LUMO+1 | 0.33259 |
| | | | | HOMO→LUMO | 0.61034 |
| S2 | 3.2397 | 382.71 | 0.0036 | HOMO-1→LUMO | 0.23652 |
| | | | | HOMO→LUMO+1 | 0.65509 |

Table S2. Excited state energy levels and orbital transitions calculated for a model of **BFTFP_*β***.

| States | Energy / eV | λ / nm | *f* / - | Orbital transitions | CI coefficient |
|---|---|---|---|---|---|
| S1 | 3.314 | 374.12 | 0.0029 | HOMO→LUMO | -0.1383 |
| | | | | HOMO→LUMO+1 | 0.69027 |
| S2 | 3.3818 | 366.62 | 0.3793 | HOMO-1→LUMO | 0.15674 |
| | | | | HOMO-1→LUMO+1 | -0.2549 |
| | | | | HOMO→LUMO | 0.62154 |
| | | | | HOMO→LUMO+1 | 0.13266 |
| S3 | 3.4581 | 358.54 | 0.0427 | HOMO-1→LUMO | 0.6803 |
| | | | | HOMO-1→LUMO+1 | 0.12862 |
| | | | | HOMO→LUMO | -0.11822 |

Table S3. Excited state energy levels and orbital transitions calculated for a model of **BFTFP_*γ*_*conformation1***.

| States | Energy / eV | λ / nm | *f* / - | Orbital transitions | CI coefficient |
|---|---|---|---|---|---|
| S1 | 3.2612 | 380.18 | 0.0743 | HOMO-1→LUMO | -0.31436 |
| | | | | HOMO-1→LUMO+1 | 0.24005 |
| | | | | HOMO→LUMO | -0.38143 |
| | | | | HOMO→LUMO+1 | 0.42737 |
| S2 | 3.2623 | 380.05 | 0.1076 | HOMO-1→LUMO | -0.2488 |
| | | | | HOMO-1→LUMO+1 | -0.30767 |
| | | | | HOMO→LUMO | 0.43232 |
| | | | | HOMO→LUMO+1 | 0.37578 |

Table S4. Excited state energy levels and orbital transitions calculated for a model of **TFPBF**_*γ*_*conformation2*.

| States | Energy / eV | λ / nm | *f* / - | Orbital transitions | CI coefficient |
|---|---|---|---|---|---|
| S1 | 3.3332 | 371.97 | 0.3828 | HOMO-1→LUMO+1 | -0.31916 |
| | | | | HOMO→LUMO | 0.61791 |
| S2 | 3.3464 | 370.5 | 0.0023 | HOMO-1→LUMO | 0.56944 |
| | | | | HOMO→LUMO+1 | -0.39184 |

Table S5. Excited state energy levels and orbital transitions calculated for a model of **BTTFP**.

| States | Energy / eV | λ / nm | *f* / - | Orbital transitions | CI coefficient |
|---|---|---|---|---|---|
| S1 | 3.1267 | 396.53 | 0.4436 | HOMO-2→LUMO | -0.13895 |
| | | | | HOMO-1→LUMO+1 | 0.28813 |
| | | | | HOMO→LUMO | 0.62117 |
| S2 | 3.1332 | 395.71 | 0.0001 | HOMO-3→LUMO | 0.13382 |
| | | | | HOMO-1→LUMO | 0.62954 |
| | | | | HOMO→LUMO+1 | 0.26897 |
| S3 | 3.3098 | 374.6 | 0.0004 | HOMO-1→LUMO | -0.27329 |
| | | | | HOMO→LUMO+1 | 0.63939 |

Table S6. Excited state energy levels and orbital transitions calculated for a model of **BFP_*α***.

| States | Energy / eV | λ / nm | *f* / - | Orbital transitions | CI coefficient |
|---|---|---|---|---|---|
| S1 | 3.1067 | 399.09 | 0.0035 | HOMO→LUMO | 0.70466 |
| S2 | 3.3888 | 365.86 | 0.0035 | HOMO-1→LUMO | 0.51296 |
| | | | | HOMO→LUMO+1 | -0.4758 |
| S3 | 3.6107 | 343.38 | 0.5638 | HOMO-1→LUMO | 0.2068 |
| | | | | HOMO-1→LUMO+1 | 0.59463 |
| | | | | HOMO→LUMO+1 | 0.31511 |

Table S7. Excited state energy levels and orbital transitions calculated for a model of **BFP_*β***.

| States | Energy / eV | λ / nm | *f* / - | Orbital transitions | CI coefficient |
|---|---|---|---|---|---|
| S1 | 3.0289 | 409.33 | 0.001 | HOMO→LUMO | 0.70503 |
| S2 | 3.3032 | 375.35 | 0.0491 | HOMO-1→LUMO | 0.55378 |
| | | | | HOMO-1→LUMO+1 | -0.1024 |
| | | | | HOMO→LUMO+1 | -0.42232 |
| S3 | 3.5231 | 351.91 | 0.0277 | HOMO-1→LUMO+1 | 0.68821 |
| | | | | HOMO→LUMO+1 | -0.15049 |

Table S8. Crystallographic and relating information for all crystals in this work.

| | **BFTFP_*α*** | **BFTFP_*β*** | **BFTFP_*γ*** | **BTTFP** | **BFP_*α*** | **BFP_*β*** | **PETFP** |
|---|---|---|---|---|---|---|---|
| CCDC dep. No. | 2420271 | 2420272 | 2420273 | 2420274 | 2420275 | 2420276 | 2420277 |
| Empirical formula | $C_{22}H_{10}F_4O_2$ | $C_{22}H_{10}F_4O_2$ | $C_{22}H_{10}F_4O_2$ | $C_{22}H_{10}F_4S_2$ | $C_{22}H_{14}O_2$ | $C_{22}H_{14}O_2$ | $C_{22}H_{14}F_4$ |
| Formula weight | 382.30 | 382.30 | 382.30 | 410.50 | 310.33 | 310.33 | 354.33 |
| Temperature [K] | 103 | 103 | 103 | 103 | 113 | 113 | 113 |
| Crystal system | monoclinic | monoclinic | triclinic | monoclinic | triclinic | monoclinic | monoclinic |
| Space group | *C*2/*c* | *Cc* | $P\bar{1}$ | $P2_1$/c | $P\bar{1}$ | $P2_1$ | $P2_1$/c |
| *a* [Å] | 17.3791(19) | 12.3696(4) | 6.0832(4) | 6.7329(6) | 5.7579(5) | 5.7690(2) | 7.8022(7) |
| *b* [Å] | 4.6272(4) | 18.8634(5) | 7.7303(4) | 6.3925(5) | 7.7062(6) | 33.1202(12) | 5.7869(4) |
| *c* [Å] | 19.4665(17) | 13.4159(4) | 17.5750(14) | 20.818(2) | 17.0414(15) | 7.7842(3) | 18.0999(17) |
| *α* [°] | 90 | 90 | 84.280(6) | 90 | 92.633(7) | 90 | 90 |
| *β* [°] | 98.682(9) | 98.178(3) | 82.761(7) | 112.145(12) | 99.613(7) | 93.360(3) | 96.941(8) |
| *γ* [°] | 90 | 90 | 73.129(6) | 90 | 92.760(7) | 90 | 90 |
| *V* [Å$^3$] | 1547.5(3) | 3098.54(16) | 782.85(9) | 829.93(15) | 743.55(11) | 1484.77(9) | 811.23(12) |
| Z | 4 | 8 | 2 | 2 | 2 | 4 | 2 |
| $\rho_{calcd}$ [g cm$^{-3}$] | 1.641 | 1.639 | 1.622 | 1.643 | 1.386 | 1.388 | 1.451 |
| Goodness of fit on $F^2$ | 1.119 | 1.085 | 1.052 | 1.118 | 1.115 | 1.076 | 1.084 |
| $R_1$ [$I \geqq 2\sigma(I)$] | 0.0496 | 0.0335 | 0.0529 | 0.0521 | 0.1143 | 0.0596 | 0.0846 |
| $wR_2$ (all data) | 0.1445 | 0.1036 | 0.1568 | 0.1357 | 0.2837 | 0.1445 | 0.2810 |
| Crystal morphology | Fiber | Block | Plate | Fiber | Plate | Plate | Plate |
| Luminescence color | Blue | Blue | Blue | Blue | Blue | Blue | Blue |

Appendix 1.

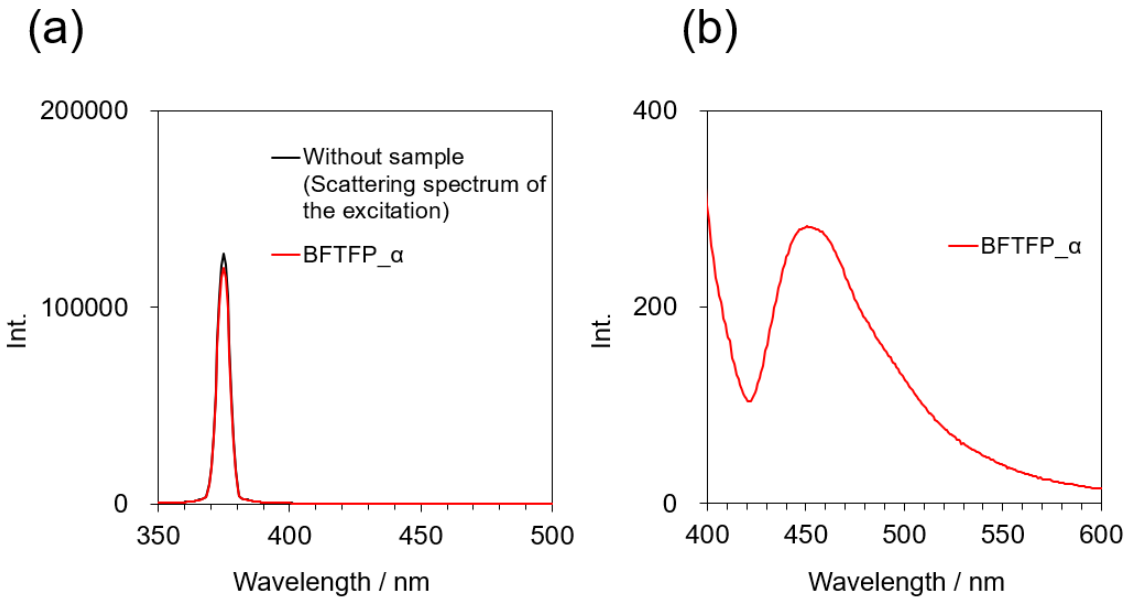


$\Phi_{PL}$ was estimated using an integrating sphere. Appendix 1-a shows scattering spectra used for the estimation. The excitation wavelength was 375 nm. Appendix 1-b shows the enlarged graphs showed in appendix 1-a. $\Phi_{PL}$ was estimated using the distraction of the intensity between the excitation scattering spectrum with and without samples, and the integrated intensity of photoluminescence. The scattering spectrum without samples and the spectrum with sample were measured at same measurement conditions.